

1 Rethinking the role of transport and photochemistry in regional 2 ozone pollution: Insights from ozone concentration and mass budgets

3 Kun Qu^{1,2,3}, Xuesong Wang^{1,2}, Xuhui Cai^{1,2}, Yu Yan^{1,2}, Xipeng Jin^{1,2}, Mihalis Vrekoussis^{3,4,5}, Jin Shen⁶,
4 Teng Xiao^{1,2}, Limin Zeng^{1,2}, and Yuanhang Zhang^{1,2,7,8}

5 ¹State Key Joint Laboratory of Environmental Simulation and Pollution Control, College of Environmental Sciences and Engineering,
6 Peking University, Beijing 100871, China

7 ²International Joint Laboratory for Regional Pollution Control, Ministry of Education, Beijing, 100816, China

8 ³Laboratory for Modeling and Observation of the Earth System (LAMOS), Institute of Environmental Physics (IUP), University of
9 Bremen, Bremen, Germany

10 ⁴Center of Marine Environmental Sciences (MARUM), University of Bremen, Germany

11 ⁵Climate and Atmosphere Research Center (CARE-C), The Cyprus Institute, Cyprus

12 ⁶State Key Laboratory of Regional Air Quality Monitoring, Guangdong Key Laboratory of Secondary Air Pollution Research, Guangdong
13 Environmental Monitoring Center, Guangzhou 510308, China

14 ⁷Beijing Innovation Center for Engineering Science and Advanced Technology, Peking University, Beijing 100871, China

15 ⁸CAS Center for Excellence in Regional Atmospheric Environment, Chinese Academy of Sciences, Xiamen 361021, China

16 *Correspondence to:* Xuesong Wang (xswang@pku.edu.cn) and Yuanhang Zhang (yhzhang@pku.edu.cn)

17 **Abstract.** Understanding the role of transport and photochemistry is essential to alleviate ambient ozone pollution. However,
18 ozone budget and source apportionment studies often report conflicting conclusions — Local photochemistry is the main cause
19 of ozone pollution based on the analyses of the former, while contrary, non-local ozone transported to the region accounts for
20 the majority in the latter results. In order to explore its potential causes, we calculated the contributions of both processes to
21 the variations of mean ozone concentration and total ozone mass (the corresponding budgets are noted as ozone concentration
22 and mass budget, respectively) within the atmospheric boundary layer (ABL) of the Pearl River Delta (PRD), China, based on
23 the modelling results of WRF-CMAQ. Quantified results show that photochemistry drives the rapid increase of ozone
24 concentrations in the daytime, whereas transport, especially the vertical exchange near the ABL top, controls the ozone mass
25 budget. The changes in transport contributions in ozone budgets indicate the influences of the ABL diurnal cycle and regional
26 wind fields, including prevailing winds and local circulations (sea breezes), on regional ozone pollution. Though transport in
27 our simulations had a relatively limited effect on ozone concentration, its high contribution to ozone mass increase in the
28 morning determined that most ozone in the PRD emanated from the outer regions. Consequently, the role of transport and
29 photochemistry in ozone pollution may differ, depending on which of the two budgets is concerned. For future studies targeting
30 ozone and other pollutants with moderately long atmospheric lifetimes, we suggest that attention should be paid to budget-
31 type selections.

32 1 Introduction

33 Since first recognized in the Los Angeles smog, ambient ozone (O_3) pollution has been a problem for many highly populated
34 urban regions around the globe (Fishman et al., 2003; Schultz et al., 2017; Fleming et al., 2018; Fowler et al., 2020).
35 Exposure to O_3 threatens human health, crop yields and ecosystems, and results in increased mortality and economic losses
36 (Mills et al., 2013; Ainsworth, 2017; Zhang et al., 2019). In addition, O_3 contributes to global warming not only directly as a
37 greenhouse gas, but also indirectly by damaging plants and suppressing land carbon sinks (Sitch et al., 2007; Naik et al.,
38 2021). Considering the above detrimental effects, efforts to reduce ambient O_3 pollution in polluted urban regions are keenly
39 required.

40

41 Understanding O_3 processes in the atmosphere is an essential prerequisite to finding effective regional O_3 control strategies.
42 Generally, high O_3 concentrations within a region are attributed to daytime photochemical production from O_3 precursors,
43 i.e. NO_x ($= NO + NO_2$) and volatile organic compounds (VOCs), under the sunlight. However, since O_3 has a moderately
44 long atmospheric lifetime (20-30 days; Stevenson et al., 2006; Bates and Jacob, 2019), the influence of dynamic processes
45 on regional-level O_3 pollution is likely to be important as well (Vilà-Guerau de Arellano et al., 2015). This can be shown by
46 the following two aspects. Firstly, O_3 is well mixed in the daytime convective atmospheric boundary layer (ABL), especially
47 during severe O_3 pollution (Zhao et al., 2019; Tang et al., 2021). Due to ABL mixing, O_3 precursors emitted by near-ground
48 sources are brought upwards to the upper ABL, where O_3 is more rapidly produced; afterwards, O_3 is transported downwards
49 to the ground (Tang et al., 2017). Therefore, to alleviate near-ground O_3 pollution, the goal should be to reduce the overall
50 O_3 level within the ABL — rather than only near the ground — based on the quantified influence of various O_3 processes
51 throughout the ABL. Secondly, transport, including horizontal transport (mainly advection) and vertical exchange near the
52 ABL top, may considerably contribute to regional O_3 pollution. More specially, through the vertical exchange in the
53 morning, O_3 in the residual layer and/or free atmosphere is entrained into the ABL, leading to the rapid increase of O_3
54 concentration after sunrise (Kaser et al., 2017; Hu et al., 2018; Zhao et al., 2019). Transported O_3 may be derived from local
55 sources, or transported from other regions, continents and even stratosphere under the combined effect of meso-, synoptic-,
56 large- and global-scale atmospheric movements (Massagué et al., 2019). In addition, O_3 precursors may also be transported
57 into the region and involved in O_3 production. These dynamic processes make the causes of regional O_3 pollution more
58 complicated than normally realized.

59

60 In previous studies, the O_3 budget was often conducted to quantify the contributions of various chemical and transport
61 processes to the variations of O_3 concentrations. For the mean O_3 concentration within the ABL ($\langle c_{O_3} \rangle$), its budget can be
62 represented as in Lenschow et al. (1981), Janssen and Pozzer (2015) and Vilà-Guerau de Arellano et al. (2015):

$$\frac{\partial \langle c_{O_3} \rangle}{\partial t} = - \left(\bar{u} \frac{\partial \langle c_{O_3} \rangle}{\partial x} + \bar{v} \frac{\partial \langle c_{O_3} \rangle}{\partial y} \right) - \frac{\partial \overline{c_{O_3}' w'}}{\partial z} + S(O_3) \quad (1)$$

63 where u , v and w indicate wind speeds in the x-, y- and z-direction, respectively. Three items on the right side of Eq. (1)
64 separately describe the contributions of 1) horizontal transport (advection), 2) vertical exchange near the ABL top, 3) gas-
65 phase chemistry, dry deposition and other processes (the term $S(\text{O}_3)$ indicates their net contributions). Reported O_3 budget
66 based on ground-based measurements (Su et al., 2018; Tan et al., 2018; Tan et al., 2019; Yu et al., 2020), aircraft-based
67 mobile observations (Lenschow et al., 1981; Trousdell et al., 2016; Trousdell et al., 2019) and Process Analysis (PA) or alike
68 modules in chemical transport models (CTMs) (Hou et al., 2014; Li et al., 2021a; Yan et al., 2021) often suggest that O_3
69 production through local photochemistry drives the noon-time increase of O_3 concentration, whereas transport reduces O_3
70 concentration over the same period. O_3 precursors are likely to be mainly derived from local emissions due to their relatively
71 short lifetimes. Thus, according to these photochemistry-dominated O_3 budget results, local emission reduction seems more
72 efficient in alleviating ambient O_3 pollution.

73

74 As an important characteristic of O_3 , O_3 source indicates from which regions and/or emission sectors O_3 originates, of which
75 the results can support effective air pollution control (Clappier et al., 2017; Thunis et al., 2019). The source apportionment of
76 ambient O_3 often suggested that most O_3 emanated from non-local sources, including the global background and emissions
77 outside the targeted regions (Guo et al., 2018; Pay et al., 2019; Liu et al., 2020). The mixing ratios of background O_3 in
78 various regions of the world are mostly within the range of 30-50 ppb (Reid et al., 2008), high enough to ensure the
79 dominance of non-local sources for O_3 pollution in less polluted regions. Since this part of O_3 is less likely to be controlled,
80 the influence of O_3 and/or precursors transport from the upwind metropolitan regions has received much attention (Lelieveld
81 et al., 2009; Boian and Andrade, 2012; Massagué et al., 2019). For regions where upwind sources notably contribute to O_3 ,
82 focusing more on emission reductions on a larger scale rather than only reducing local emissions is needed to effectively
83 control O_3 pollution. One successful example is the establishment of the “Ozone Transport Region” in the north-eastern US
84 by the US Environmental Protection Agency, which promoted collaborative emission reductions among states to address
85 inter-state O_3 transport (Novel, 1992). In China, O_3 pollution was overall more severe than in other countries recently (Lu et
86 al., 2018). Since high pollutant emissions are widely distributed in East China, the so-called “gigacity” (Kulmala et al.,
87 2021), upwind emissions often contribute more to O_3 pollution in the major city clusters compared to local emissions, as
88 suggested by O_3 source studies in China (Liu et al., 2020). Therefore, transport seems to play a more important role in
89 ambient O_3 pollution here as well, and the efforts of joint prevention and control among regions to reduce O_3 levels are
90 necessary (Li et al., 2021b). Apparently, insights from O_3 source apportionment differ from the conclusions based on the O_3
91 budgets.

92

93 Simulations by Eulerian CTMs are capable of reproducing O_3 processes within the ABL. However, since the contribution of
94 vertical exchange near the ABL top is not specifically quantified in normally used ABL parameterizations, it cannot be
95 directly provided by the PA module but requires additional calculations (Kaser et al., 2017). Thus O_3 budget within the ABL
96 on the hourly scale is seldom reported based on CTMs results. In this study, we constructed the post-processing tool

97 *flux_4d_cal* to quantify the contributions of O₃ processes, including gas-phase chemistry, horizontal transport and vertical
 98 exchange near the ABL top, in the O₃ budget within the ABL of the targeted region. The calculations were conducted based
 99 on the simulation results from the Weather Research and Forecasting (WRF) and Community Multiscale Air Quality
 100 (CMAQ) models, of which the details are briefly introduced in Sect. 2. To explore the reasons behind the contradictory
 101 views on the role of transport and photochemistry in regional ozone pollution between the O₃ budget in Eq. (1) and O₃
 102 source apportionment, the other type of O₃ budget, the O₃ mass budget, was introduced by this tool. It aims to identify the
 103 contributions of O₃ processes to the variation of total O₃ mass within the ABL (m_{O_3}) and is written as:

$$\frac{\partial m_{O_3}}{\partial t} = -(\bar{u}s_x\langle c_{O_3} \rangle + \bar{v}s_y\langle c_{O_3} \rangle) - \overline{c_{O_3}'w'}s_z + S(O_3)V \quad (2)$$

104 where s_x , s_y , s_z are the areas of the interfaces in the x-, y- and z-direction, respectively, and V is the volume of the ABL
 105 column. Regional-level O₃ mass budget can be applied to illustrate better the changes in regional O₃ sources and their
 106 influencing factors (more in-detail discussions are given in Sect. 2.4). The O₃ budget shown in Eq. (1) is hereinafter re-
 107 defined as the O₃ concentration budget, which focuses on the contributions of O₃ processes to the variation of ABL-mean O₃
 108 concentration. Moreover, based on the O₃ mass budgets in the sensitivity scenarios that zeroes out emissions in specific
 109 regions, the regional source of O₃ mass change contributed by different processes can also be identified. The Pearl River
 110 Delta (PRD) region, a city cluster located on the southeast coast of China and exposed to severe O₃ pollution in summer and
 111 autumn (Gao et al., 2018), was selected as the targeted region in this study. The quantified results of O₃ concentration and
 112 mass budgets in the PRD illustrated the complex effects of O₃ processes, especially transport, on regional O₃ pollution, and
 113 revealed that the distinct views on the role of photochemistry and transport are possibly linked to the differences between
 114 two O₃ budgets.

115 2 Methodology: O₃ budget calculations and model setup

116 2.1 Processes in O₃ budgets

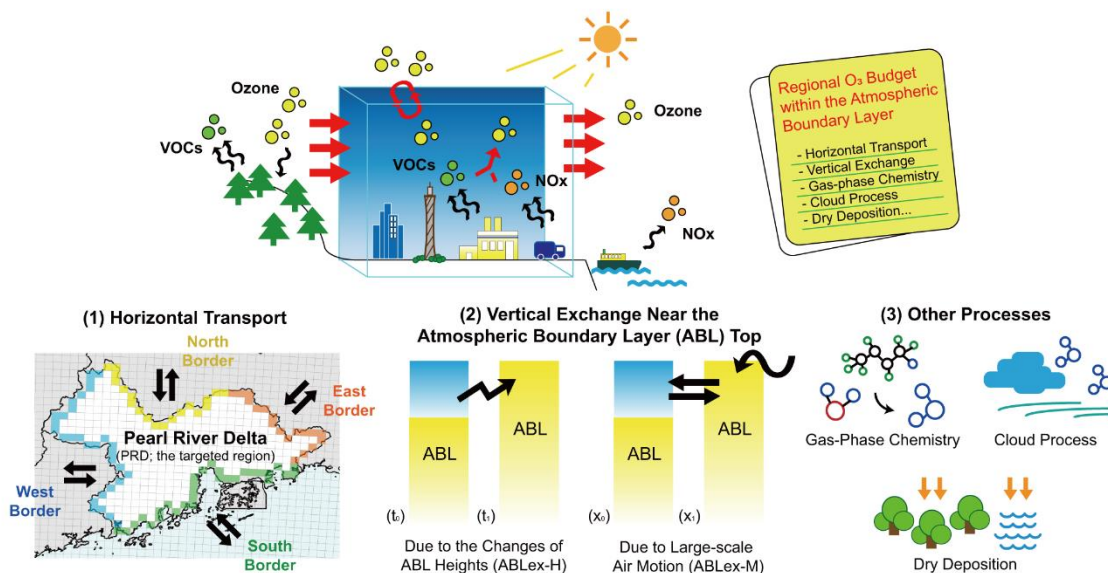
117 Figure 1 displays all processes considered in the calculation of O₃ budgets as well as the distributions of the PRD grids
 118 (lower-left panel; defined as the grids within the PRD), which include the border grids (defined as the PRD grids adjacent to
 119 the outer regions) and non-border grids.

120

121 Horizontal transport through the borders of the PRD in four directions and vertical exchange near the ABL top are the
 122 transport processes concerned in this study. For the latter, its contribution in the O₃ concentration budget (the second item on
 123 the right side of Eq. (1)) is quantified by Sinclair et al. (2010) and Jin et al. (2021):

$$-\frac{\partial \overline{c_{O_3}'w'}}{\partial z} = -\frac{\Delta c_{O_3}}{H} \frac{\partial H}{\partial t} - \frac{\Delta c_{O_3}}{H} \left(u_h \frac{\partial H}{\partial x} + v_h \frac{\partial H}{\partial y} - w_h \right) \quad (3)$$

124 where H is the ABL height; Δc_{O_3} is the difference between O_3 concentrations above and within the ABL; u_h , v_h and w_h are
 125 the ABL-top wind speeds in the x, y and z-direction, respectively. Items on the right side of Eq. (3) suggested that the
 126 occurrence of vertical exchange is attributed to 1) the temporal changes of ABL heights and 2) large-scale air motion
 127 (advection) perpendicular to the ABL top and its slope. Their contributions can be identified in the O_3 mass budget as well,
 128 of which the details are introduced in Sect 2.2. Hereafter, vertical exchanges due to the above two processes are marked as
 129 ABLex-H and ABLex-M, respectively. The contributions of all transport processes were quantified using meteorological
 130 parameters and O_3 concentrations modelled by WRF-CMAQ. The basic calculations of the above contributions in the O_3
 131 concentration and mass budgets are separately introduced in the following two sections, and details about the calculation
 132 process are presented in Text S1.
 133



134
 135 **Figure 1.** Schematic illustration of regional O_3 budgets (the upper panel) and processes considered (the lower panel): (1) Horizontal
 136 transport through the borders of the Pearl River Delta (PRD) in four directions (the distributions of the PRD grids are also shown: yellow,
 137 green, blue, orange for the north, south, west and east border grids, respectively, and white for the non-border grids); (2) Vertical exchange
 138 near the atmospheric boundary layer (ABL) top, including the process due to the changes of ABL heights (ABLex-H) and large-scale air
 139 motion (ABLex-M); (3) Other processes, including gas-phase chemistry, cloud process and dry deposition in this study.

140
 141 Other processes in O_3 budgets include gas-phase chemistry (including daytime photochemical O_3 production and O_3 titration
 142 by NO), cloud process (including below and in-cloud mixing, aqueous-phase chemistry, wet deposition; Liu et al., 2011) and
 143 dry deposition. Their contributions are calculated based on the output of the PA module in CMAQ (for a more detailed
 144 description of calculations, see Text S1). Since diffusion near the boundaries and top of the region is expected to have a
 145 minor influence on the variation of O_3 concentration and mass, we did not involve this process in the quantifications.

146 2.2 Transport contributions in the O₃ mass budget

147 The method by Yang et al. (2012) and Chang et al. (2018) was applied to quantify the contributions of horizontal transport in
 148 the O₃ mass budget. For instance, the contribution of the advection through the west/east interface of a grid cell column
 149 within the ABL to total O₃ mass (F_{htrans}) in the column during the time interval dt is calculated as:

$$F_{htrans} = \int_0^H c_{O_3} u L dz dt \quad (4)$$

150 where L is the width of the grid cell (equal to the horizontal resolution of the model); dz is the height of vertical layers. For
 151 advection through the north/south interface, the calculation is similar to Eq. (4), except for using v instead of u . F_{htrans}
 152 values through every interface between one type of border and the outer region were summed up as the net contribution of
 153 horizontal transport through that border in the O₃ mass budget.

154

155 Following Sinclair et al. (2010) and Jin et al. (2021), the contribution of vertical exchange near the ABL top to O₃ mass
 156 (F_{ABLex}) during the time interval dt can be expressed as:

$$F_{ABLex} = F_{ABLex-H} + F_{ABLex-M} = c_{O_3-h} \frac{\partial H}{\partial t} L^2 dt + c_{O_3-h} \left(u_h \frac{\partial H}{\partial x} + v_h \frac{\partial H}{\partial y} - w_h \right) L^2 dt \quad (5)$$

157 where c_{O_3-h} is the O₃ concentration at the ABL top. Two terms on the right-most side of Eq. (5) separately describe the
 158 contributions of ABLex-H and ABLex-M (denoted separately as $F_{ABLex-H}$ and $F_{ABLex-M}$). F_{ABLex} values in all the PRD grids
 159 were summed up as the net contribution of vertical exchange near the ABL top in the O₃ mass budget.

160 2.3 Transport contributions in the O₃ concentration budget

161 For one or limited grid columns, it is possible to directly use Eq. (1) to quantify the O₃ concentration budget based on CTMs
 162 results. But for the ABL of the PRD, which comprises over 260 grid columns, such calculations could easily become over-
 163 complicated. Therefore, a different approach was applied to calculate the regional-level O₃ concentration budget.

164

165 Suppose that air parcels with a total volume of dV are transported into the ABL of the PRD (its original volume is V) during
 166 the time interval dt . For horizontal transport, the variation of $\langle c_{O_3} \rangle$ under its influence ($d\langle c_{O_3} \rangle_{htrans}$) can be written as:

$$d\langle c_{O_3} \rangle_{htrans} = \frac{F_{htrans} + \langle c_{O_3} \rangle (V - dV)}{V} - \langle c_{O_3} \rangle = \frac{F_{htrans} - \langle c_{O_3} \rangle dV}{V} \quad (6)$$

167

168 Since ABLex-M is also an advection process, its contribution in the O₃ concentration budget ($d\langle c_{O_3} \rangle_{ABLex-M}$) can be
 169 quantified using a similar formula, except for using $F_{ABLex-M}$ instead of F_{htrans} .

170

171 Through ABLex-H, air parcels in the residual layer and/or free atmosphere are merged into (or segmented out of) the ABL.

172 Thus, the variation of $\langle c_{O_3} \rangle$ under its influence ($d\langle c_{O_3} \rangle_{ABLex-H}$) is expressed as:

$$d\langle c_{O_3} \rangle_{ABLex-H} = \frac{F_{ABLex-H} + \langle c_{O_3} \rangle V}{V + dV} - \langle c_{O_3} \rangle = \frac{F_{ABLex-H} - \langle c_{O_3} \rangle dV}{V + dV} \quad (7)$$

173

174 If the targeted region was small enough, Eqs. (6) and (7) would have the same forms as the corresponding items in Eq. (1),
175 confirming the applicability of the above calculations (for details, see Text S2). All variables in Eqs. (6) and (7) can be
176 quantified by the post-processing tool, making the method suitable for calculating the regional-scale O_3 concentration
177 budget.

178

179 However, due to the prominent diurnal cycle of ABL, V in Eqs. (6) and (7) may change notably within an hour, leading to
180 bias in the hourly estimations of $d\langle c_{O_3} \rangle_{htrans}$, $d\langle c_{O_3} \rangle_{ABLex-H}$ and $d\langle c_{O_3} \rangle_{ABLex-M}$ when using V at the start and end of the
181 hour. In order to reduce this potential bias, we designed two calculation paths (Fig. S1):

- 182 • O_3 mass change \rightarrow ABL volume change
- 183 • ABL volume change \rightarrow O_3 mass change

184 where only O_3 mass or ABL volume changes in each calculation step. The contribution of ABLex-H can be decomposed into
185 two parts: ABL volume change due to ABL development (collapse) leads to lower (higher) O_3 concentration, and O_3
186 transported into (out of) the ABL through ABLex-H leads to O_3 increase (decrease). These contributions are quantified
187 separately in the ABL volume and O_3 mass change step. The contributions of other processes are quantified only in the O_3
188 mass change step. For one process, its contribution to the variation of O_3 concentration is calculated through both paths, and
189 the mean value of two results serves as an estimation close to its real contribution in the O_3 concentration budget.

190 2.4 Difference between two O_3 budgets

191 Suppose that the mean O_3 concentration in the transported air parcels is $\langle c_{O_3} \rangle_{trans}$. For horizontal transport, its contributions
192 in the O_3 mass and concentration budgets can be separately written as:

$$F_{htrans} = \langle c_{O_3} \rangle_{trans} dV \quad (8)$$

$$d\langle c_{O_3} \rangle_{htrans} = \frac{dV}{V} (\langle c_{O_3} \rangle_{trans} - \langle c_{O_3} \rangle) \quad (9)$$

193 Apparently, F_{htrans} is related to the O_3 concentrations in the transported air parcels, but not to those in the targeted region. It
194 indicates how much O_3 is transported into or out of the region. Whether it is positive or negative only depends on the
195 direction of transport — O_3 being transported into (out of) the region leads to the increase (decrease) of O_3 mass, which
196 corresponds to a positive (negative) contribution in the O_3 mass budget. In contrast, $d\langle c_{O_3} \rangle_{htrans}$ quantifies how much
197 horizontal transport alters regional-mean O_3 levels. As shown in Eq. (9), it is linked to the difference between O_3
198 concentrations in the transported air parcels and the targeted region. O_3 being transported into (out of) the region does not

necessarily result in a higher (lower) O₃ concentration. For instance, when clean air parcels with relatively low O₃ levels are transported into the region, they dilute O₃ pollution and reduce O₃ concentration ($d\langle c_{O_3} \rangle_{htrans} < 0$). These effects are the same for ABLex-H and ABLex-M, also showing the above difference between the two O₃ budgets.

To understand the influence of various processes on O₃ sources, it is required to identify the sources of “new O₃” into the region and “disappeared O₃” out of the region contributed by processes, rather than how these processes lead to the variations of O₃ concentration. According to the above discussions, the O₃ mass budget is suitable to explain how transport and photochemistry determine the regional sources of O₃ in this study.

2.5 Model setup and validation

The O₃ concentration and mass budgets within the ABL of the PRD were calculated based on the WRF-CMAQ modelling results by Qu et al. (2021). In the models, two nested domains with the resolution of 36 and 12 km were set (denoted as d01 and d02 hereafter), and results in the finer d02 were used in the calculations of O₃ budgets. October 2015 (October 11–November 10, 2015) and July 2016 (July 1–31, 2016) were selected as the representative months in autumn and summer, respectively, for the PRD. Here, O₃ polluted days are defined when the maximum hourly O₃ concentrations exceed 200 µg/m³, or the maximum 8-hour average O₃ concentrations exceed 160 µg/m³ (both are the Grade-II O₃ thresholds in the Chinese National Ambient Air Quality Standard) in any municipality of the PRD. According to this definition, there were 16 and 12 O₃ polluted days in the two months, respectively (more information is given in Table S1). Further discussions focus on O₃ budgets during these days. The detailed setup of WRF-CMAQ, the validation of modelled meteorological parameters, O₃, NO₂ concentrations and hydrocarbons mixing ratios have been introduced by Qu et al. (2021). In this study, we also compared modelled ABL height, the vertical profiles of wind speed, direction and O₃ mixing ratio in Hong Kong (located in the south PRD) with corresponding observations from the IAGOS (In-service Aircraft for a Global Observing System; Petzold et al., 2015) dataset. As presented in Text S3, the acceptable modelling performance of these parameters indicates that the model provides reasonable initial data for the O₃ budget calculations.

If the calculation methods and assumptions were reasonable, the budget closure, or

$$\frac{\partial \langle c_{O_3} \rangle (or m_{O_3})}{\partial t} - (S_{htrans} + S_{ABLex} + S_{chem} + S_{cloud} + S_{ddep}) = 0 \quad (10)$$

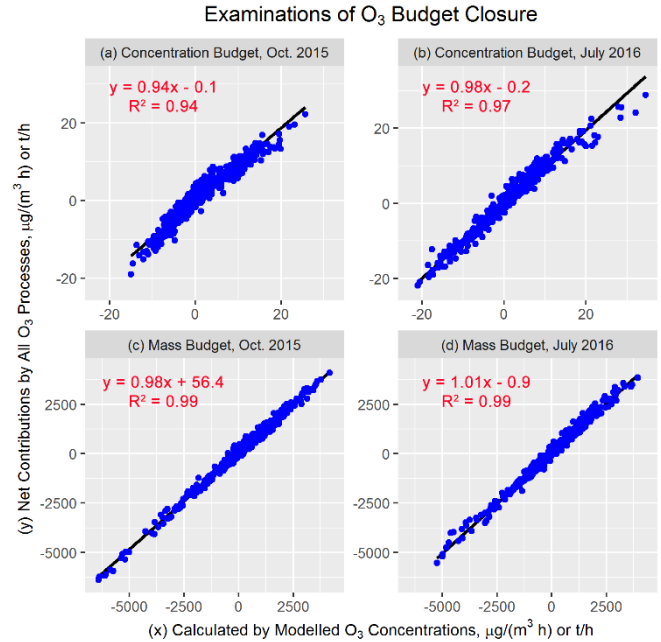
would be achieved (S_{htrans} , S_{ABLex} , S_{chem} , S_{cloud} and S_{ddep} indicate the contributions of horizontal transport, vertical exchange near the ABL top, gas-phase chemistry, cloud process and dry deposition, respectively, in O₃ budgets). Therefore, we used Eq. (10) to examine the validity of the calculations. Total O₃ masses at the start and end of each hour were directly used to calculate the hourly variations of O₃ mass ($\frac{\partial m_{O_3}}{\partial t}$). Besides these, volumes at these two moments (calculated using ABL heights in all the PRD grids) were also needed to calculate the hourly variations of O₃ concentration ($\frac{\partial \langle c_{O_3} \rangle}{\partial t}$). The

229 contributions of various processes in the O₃ concentration and mass budgets were provided by the post-processing tool. As
230 displayed in Fig. 2, hourly variations of O₃ concentration/mass and the corresponding net contributions from all processes
231 show good correlations ($R^2 > 0.9$), with all fitted lines being close to the 1:1 line. Thus, the closure is met for the two O₃
232 budgets in both months, allowing for further analyses based on the quantified budgets.

233 **2.6 Identifying regional sources of O₃ mass changes contributed by various processes**

234 It is generally believed that transport (gas-phase chemistry) is closely linked to the contributions of non-local (local)
235 emissions for O₃, but quantitative evaluation of the connections between O₃ processes and sources is still understudied. By
236 combining O₃ budget calculations with the source apportionment method, the Brute Force Method (BFM; Clappier et al.,
237 2017), we identified the regional sources of O₃ mass changes contributed by transport and gas-phase chemistry. Of interest
238 were the contributions of emissions in the PRD, other regions within d02 (mainly East and Central China, short for EC-
239 China), and regions outside d02 (the boundary conditions (BCON) of d02 modelling). The distributions of these regions are
240 shown in Fig. S2. Besides the base scenario, three sensitivity scenarios were simulated:

- 241 • The PRD_zero scenario: Emissions in the PRD were zeroed out;
- 242 • The EC-China_zero scenario: Emissions in the EC-China were zeroed out;
- 243 • The All_zero scenario: All emissions within d02 were shut down.



244
245 **Figure 2.** The examinations of O₃ budget closure in Oct. 2015 (a,c) and July 2016 (b,d) for the hourly O₃ concentration budget (a-b) and
246 mass budget (c-d). The units for the O₃ concentration and mass budgets are $\mu\text{g}/(\text{m}^3 \text{ h})$ and t/h , respectively. The solid black lines in the
247 plots are the fitted lines.

For the process i , its hourly contributions in the O_3 mass budget in the base scenario and three sensitivity scenarios were quantified using the same method introduced in Sect. 2.2, which are marked as $f_{i,base}$, f_{i,PRD_zero} , $f_{i,EC-China_zero}$, and f_{i,all_zero} , respectively. Then, the contributions of PRD, EC-China and BCON in O_3 mass changes attributed to the process i (separately denoted as $F_{i,PRD}$, $F_{i,EC-China}$, and $F_{i,BCON}$) were calculated as follows:

$$F_{i,PRD} = \frac{1}{2}[(f_{i,base} - f_{i,PRD_zero}) + (f_{i,EC-China_zero} - f_{i,all_zero})] \quad (11)$$

$$F_{i,EC-China} = \frac{1}{2}[(f_{i,base} - f_{i,EC-China_zero}) + (f_{i,PRD_zero} - f_{i,all_zero})] \quad (12)$$

$$F_{i,BCON} = f_{i,all_zero} \quad (13)$$

In Eqs. (11) and (12), the contributions of emissions are calculated as the average results of these using top-down BFM ($(f_{i,base} - f_{i,PRD_zero})$, $(f_{i,base} - f_{i,EC-China_zero})$) for the PRD and EC-China emissions, respectively) and bottom-up BFM ($(f_{i,EC-China_zero} - f_{i,all_zero})$, $(f_{i,PRD_zero} - f_{i,all_zero})$) for the PRD and EC-China emissions, respectively). By doing so, the non-additivity (the sum of all contributions is not equal to the concerned metric) caused by the non-linearity between O_3 and precursors can be avoided (Qu et al., 2021).

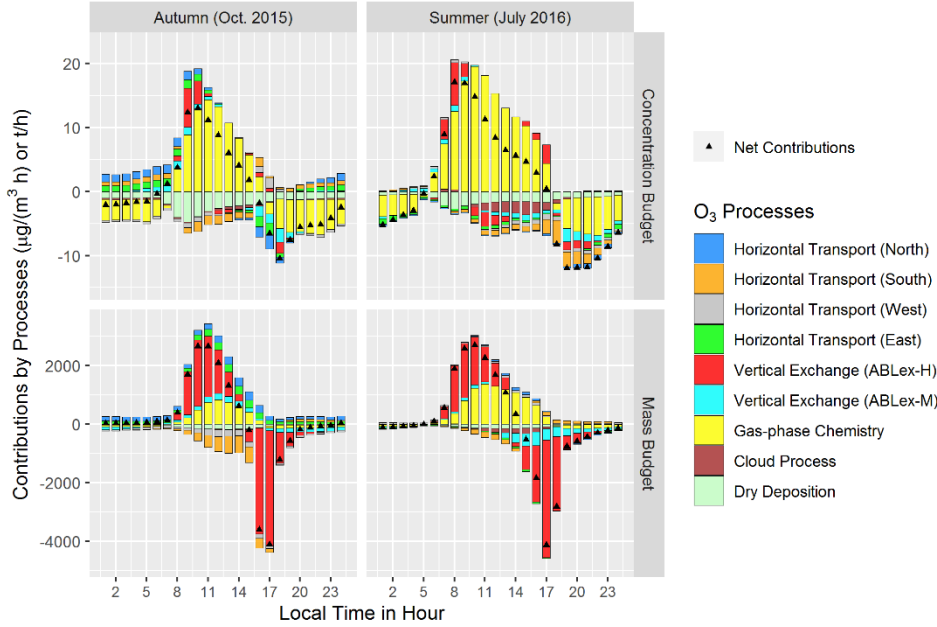
3 Results

3.1 O_3 concentration budget

The upper panels of Fig. 3 show the diurnal changes of the O_3 concentration budget within the ABL of the PRD. According to the net contributions, O_3 concentration increased during most hours in the daytime, and its reduction at night was also considerable. We also compared the diurnal changes of ABL-mean O_3 concentration with those of observed and modelled mean near-ground O_3 concentrations in 18 sites of the Guangdong-Hong Kong-Macao PRD Regional Air Quality Monitoring Network (distributions are shown in Fig. S3). As presented in Fig. S4, three types of O_3 diurnal changes display similar characteristics. However, the budget of ABL-mean O_3 concentration can better reveal the influences of transport and photochemistry on the overall O_3 levels as well as the general causes of O_3 pollution in the targeted region. Such results in the PRD are discussed in the following.

Apparently, gas-phase chemistry controlled almost exclusively the O_3 concentration budget. During the morning hours, which are defined as the period from sunrise (~6:00 local time (LT) in autumn, ~5:00 LT in summer) to the O_3 -peak hour (~14:00 LT), it (photochemistry) contributed to, on average, 74% and 95% of the O_3 concentration increase in autumn and summer, respectively. These contributions are notably higher than transport contributions (25% in autumn, 5% in summer). Gas-phase chemistry also led to the decrease of O_3 concentration at night, suggesting the impact of O_3 titration by emitted NO. It does not mean that the influence of transport on O_3 concentration can be neglected every hour. Considerable contributions of transport (mainly by ABLex-H) to O_3 increase are found 2-3 hours after sunrise, with the highest hourly

275 mean contributions reaching ~40% and ~25% in autumn and summer, respectively. It indicates the notable influences of air
 276 masses containing high-level O₃ entrained from residual layers. ABLex-M and horizontal transport may contribute to the
 277 increase or decrease of ABL-mean O₃ concentration, depending on the O₃ levels in air parcels transported into and out of the
 278 region (more analyses are given in Sect. 3.4). But overall, these two processes had only limited contributions to the
 279 variations of O₃ concentration. Dry deposition contributed to a considerable decrease in O₃ concentration, especially in the
 280 daytime, and served as the major sink process for O₃. To summarize, the results of the O₃ concentration budget indicate that
 281 gas-phase chemistry played a major role in the variations of O₃ concentrations in the PRD. In particular, photochemistry led
 282 to the rapid formation of O₃ pollution in the daytime, rather than transport. Our conclusions agree well with those in previous
 283 publications on the O₃ concentration budget (Lenschow et al., 1981; Hou et al., 2014; Trousdell et al., 2016; Su et al., 2018;
 284 Tan et al., 2018; Tan et al., 2019; Trousdell et al., 2019; Yu et al., 2020; Li et al., 2021a; Yan et al., 2021).
 285



286
 287 **Figure 3.** Mean diurnal changes of the O₃ concentration budget (the upper panels) and mass budget (the lower panels) on the polluted days
 288 of representative months in autumn (Oct. 2015; left panels) and summer (July 2016; right panels) within the atmospheric boundary layer of
 289 the Pearl River Delta. The units for the O₃ concentration and mass budgets are $\mu\text{g}/(\text{m}^3 \text{ h})$ and t/h , respectively.

290 3.2 O₃ mass budget

291 The total O₃ mass within the ABL of the PRD increased during the morning hours, then decreased rapidly in the afternoon
 292 and remained stable at night in both autumn and summer (Fig. 3, the lower panels). The change of total O₃ mass agrees well
 293 with the ABL diurnal cycle (Lee, 2018) — daytime ABL development (collapse) and notable O₃ mass increase (decrease)
 294 almost occurred simultaneously, and the negligible changes in O₃ mass at night may be linked to the small variations of
 295 stable ABL.

296

297 The contribution of processes in the O₃ mass budget highlights the prominent role of transport. On average, it contributed to
298 78% and 53% of O₃ mass increase during the morning hours in autumn and summer, respectively, and over 90% of O₃ mass
299 decrease during the afternoon hours of both seasons (defined as 14:00-19:00 LT in autumn and 14:00-20:00 LT in summer).
300 Most O₃ was transported into or out of the PRD through the vertical exchange near the ABL top, especially ABLex-H, which
301 explains the consistency between the changes of O₃ mass and ABL. The influences of ABLex-M and horizontal transport on
302 O₃ mass were relatively limited. However, they indicated well the characteristics and variations of regional wind fields (more
303 details are given in the next section). Gas-phase chemistry (photochemistry) also contributed to the increasing O₃ mass
304 during the daytime, especially in summer. However, its mean contributions during the morning hours (22% in autumn, 47%
305 in summer) were lower than those of transport. In addition, cloud process and dry deposition acted as O₃ sinks with
306 negligible contributions to O₃ mass. Based on the above discussions, transport tends to be more important than
307 photochemistry in the O₃ mass budget, which differs from the conclusions of the O₃ concentration budget.

308

309 The O₃ mass budget in this study overall agrees well with our common understanding of O₃ processes. The main role of
310 transport (the vertical exchange near the ABL top) in the O₃ mass budget reflects the influence of the ABL diurnal cycle on
311 regional O₃ pollution. Specifically, despite of relatively lower influence on O₃ concentration increase in comparison to that
312 of photochemistry, massive O₃ being transported into the ABL during the morning hours nearly determines the regional
313 sources of O₃ pollution. Quantified results combining O₃ mass budget and source apportionment are further discussed in
314 Sect. 3.4.

315 **3.3 Influences of regional wind fields on transport contributions in O₃ budgets**

316 Through the contributions of horizontal transport and ABLex-M in O₃ budgets, the characteristics and variations of regional
317 wind fields, including the prevailing winds and local circulations (sea breezes), can also be identified. Two main findings in
318 this study are presented as follows:

319

320 (1) The contributions of horizontal transport and ABLex-M in autumn suggest the characteristics of prevailing winds in the
321 PRD.

322

323 Northerly and easterly winds prevail in autumn (as indicated by the wind roses in Fig. S5). Thus, correspondingly, O₃ was
324 transported into the PRD through its north and east borders, out of the PRD through the south and west borders, as shown in
325 the O₃ mass budget (Fig. 3). O₃ masses transported out of the region were generally higher than those transported into the
326 region in the daytime, which is attributed to higher downwind O₃ levels due to O₃ production from local emissions. “Low O₃
327 in, high O₃ out” also explains why horizontal transport led to the net decrease of O₃ concentration in the daytime. At night,
328 O₃ was still transported into the region through the north and east borders of the PRD, but these processes became important

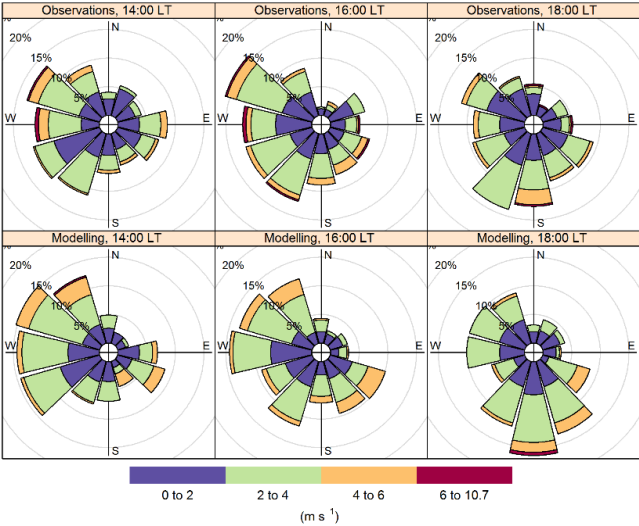
329 O₃ sources based on the O₃ concentration budget. This is to say, with relatively high O₃ levels compared to the NO_x-titrated
 330 urban atmosphere, air parcels transported from the upwind outskirts helped maintain night-time O₃ levels in the PRD to
 331 some extent.
 332
 333 The daytime contributions of ABLex-M in the O₃ mass budget also indicate the effects of prevailing northerly winds. The
 334 PRD has mountainous regions in the northern, western and eastern outskirts, as well as urban regions with lower altitudes in
 335 the central plain. Thus, the positive contributions of ABLex-M through the ABL top (in the z-direction) can be found in
 336 mountainous regions (Fig. S6a-b), suggesting north winds resulted in the downward transport of O₃ along the terrain.
 337 Daytime ABL heights in urban regions were, in general, higher than those in mountainous regions, which is the other reason
 338 why O₃ can be transported through the ABL slope (in the x-/y-direction) near the urban-rural interfaces when north wind
 339 prevailed (Fig. S6c-d). For the O₃ concentration budget, ABLex-M contributed to the increase of O₃ concentration during
 340 several hours after sunrise but the decrease of O₃ concentration in the afternoon. This different effect is attributed to different
 341 comparison results between ABL and above-ABL mean O₃ concentrations in the two periods (ABL < above-ABL in the
 342 morning, ABL > above-ABL in the afternoon; Fig. S7).
 343
 344 (2) The contributions of horizontal transport and ABLex-M in summer indicate the influence of sea breezes in the PRD.
 345
 346 Although southerly winds normally prevail in summer in the PRD (Fig. S5), on O₃ polluted days, air parcels from other
 347 directions could potentially influence the region as well (Qu et al., 2021). Thus the mean contribution of horizontal transport
 348 to O₃ mass in summer was lower than those in autumn. What interests us more is the different contributions of horizontal
 349 transport through the south border before and after ~14:00 LT, as indicated by the results of the O₃ mass budget. Two O₃
 350 budgets also suggest high O₃ mass and concentration decreases contributed by ABLex-M in the afternoon. These phenomena
 351 are both related to the influence of sea breezes.
 352
 353 Figure 4 shows the near-ground wind roses at 14:00, 16:00 and 18:00 LT of O₃ polluted days in July 2016 based on the
 354 observational and modelling results in national meteorological sites within the PRD. At 14:00 LT, the main wind directions
 355 were W, SW and NW in both datasets. More S and SE winds occurred in later hours, and they became the prevailing winds
 356 at 18:00 LT — suggesting the gradual development of sea breezes in the PRD. Thus, O₃ was originally transported out of the
 357 PRD through the south border with negative contributions to O₃ mass; in the late afternoon, sea breezes reversed the
 358 directions of O₃ transport, resulting in positive contributions to O₃ mass by horizontal transport through the south border
 359 (Fig. 3). Moreover, sea breezes are connected to the changes of not only horizontal wind fields, but also vertical wind fields.
 360 Take the O₃ polluted day July 24th, 2016 for example, and the cross-section of O₃ concentrations and wind fields in the PRD
 361 at 16:00 LT is shown in Fig. 5 (the cross-section is made along the 113.2° E longitude, ranging from 26.0 to 20.0° N in
 362 latitude). Strong southerly wind and lower O₃ concentrations are found in the southern PRD, indicating the influence of sea

363 breezes on the region during that time. Near the interfaces where sea breezes encountered local air parcels (indicated by the
 364 drastic increase in O_3 levels from less than $100 \mu\text{g}/\text{m}^3$ to about $100\text{--}150 \mu\text{g}/\text{m}^3$), updrafts occurred, suggesting the formation
 365 of sea breeze front (Ding et al., 2004; You and Fung, 2019). It promoted the upward transport of O_3 from the ABL, or
 366 considerable O_3 mass decrease attributed to ABLex-M. The above influences of sea breezes can also be found in autumn but
 367 were weaker and occurred later.

368

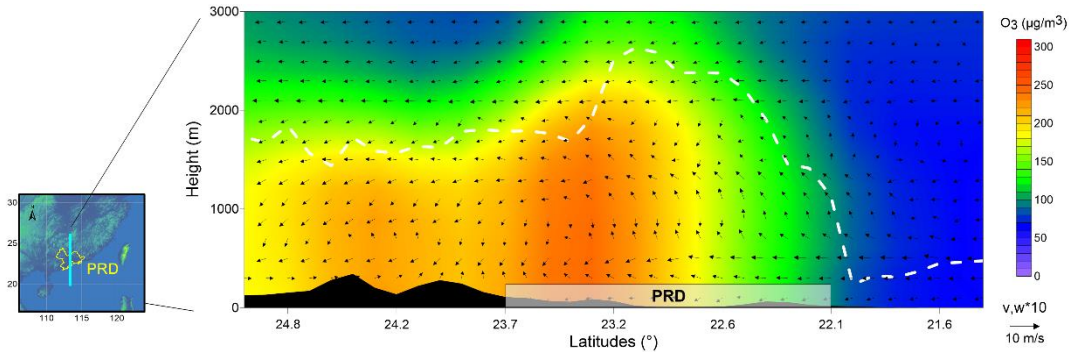
369 Through the calculations and analyses of O_3 budgets, the contributions of complex transport processes in multiple scales to
 370 O_3 concentration and mass were quantified. These results can help us gain a deeper understanding of how transport
 371 influences regional O_3 pollution in the PRD.

372



373

374 **Figure 4.** Wind roses at 14:00, 16:00, and 18:00 local time (LT) of the O_3 polluted days in July 2016 in the Pearl River Delta (PRD).
 375 Observational and modelling wind speeds and directions in 29 national meteorological sites within the PRD were used for this figure.

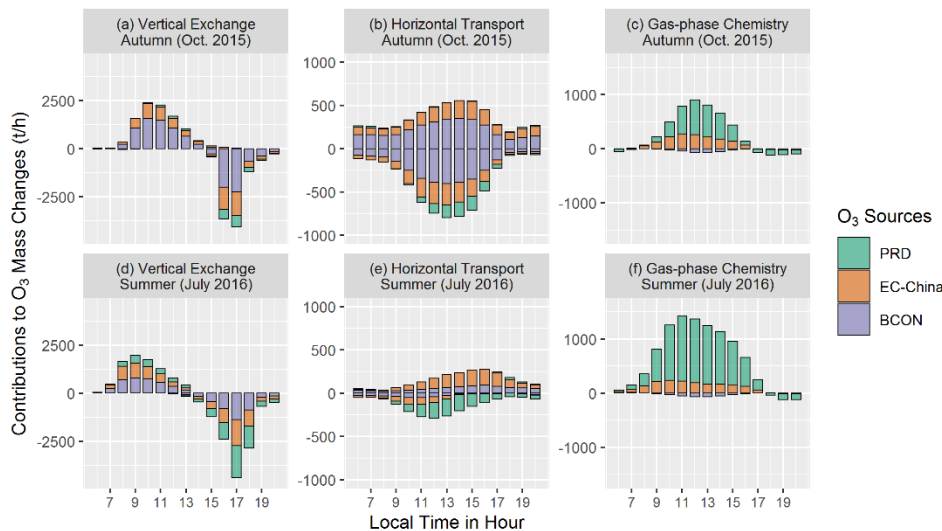


376

377 **Figure 5.** Cross-section of O_3 concentrations ($\mu\text{g}/\text{m}^3$) and wind fields at 16:00 local time on July 24th, 2016. The dashed white line
 378 indicates the top of the atmospheric boundary layer. PRD, Pearl River Delta.

379 **3.4 Regional sources of O₃ mass changes contributed by transport and photochemistry**

380 Based on previous publications (Li et al., 2012; Li et al., 2013; Yang et al., 2019; Gao et al., 2020), non-local sources often
381 contributed to most O₃ in the PRD. This outcome is also true for the O₃ polluted days in the representative months of autumn
382 and summer in this study, when non-local sources contributed on average to 89% and 65% of the O₃ in the PRD,
383 respectively, in 9:00-17:00 LT (55% and 32% contributed by BCON, 34% and 33% contributed by EC-China in two months;
384 Qu et al., 2021). To explain why non-local O₃ sources are dominant in the PRD, we identified the regional sources of O₃
385 mass changes contributed by the vertical exchange near the ABL top, horizontal transport and gas-phase chemistry (Fig. 6;
386 the results in 5:00-20:00 LT are shown). Since the O₃ mass decrease overall showed similar regional sources as O₃ within the
387 region, further analyses focus on the regional sources of O₃ mass increase, that is, O₃ transported into and produced within
388 the PRD.
389



390
391 **Figure 6.** The regional sources of hourly O₃ mass changes contributed by (a,d) vertical exchange near the ABL top, (b,e) horizontal
392 transport, and (c,f) gas-phase chemistry on the polluted days of representative months in autumn (Oct. 2015; a-c) and summer (July 2016;
393 d-f). The results within 5:00-20:00 LT are shown here. PRD, Pearl River Delta; EC-China, East and Central China; BCON, the boundary
394 conditions of d02 modelling, or the contribution of sources outside d02.

395
396 Through the vertical exchange near the ABL top, the process with the most notable contributions in the O₃ mass budget,
397 massive non-local O₃ entered into the ABL of the PRD. In the morning-hour O₃ mass increase attributed to the process,
398 BCON and EC-China accounted for 65% and 31%, respectively, in autumn. By contrast, local emissions only contributed to
399 4% in this transported O₃ during the same period, suggesting that local O₃ recirculation had only a limited influence on O₃
400 pollution. The results in summer were similar to those in autumn, except that the contributions of PRD (local) and EC-China
401 emissions were higher in O₃ transported into the region through vertical exchange. In particular, local contribution accounted

for 20% in the transported O₃ during the morning hours, but was still lower than non-local contribution (38% and 42% for EC-China and BCON, respectively).

O₃ mass increase attributed to horizontal transport was connected to the contribution of non-local sources as well. In both seasons, O₃ transported into the PRD originated almost all from non-local sources.

It is not surprising that most O₃ produced through gas-phase chemistry (photochemistry) was related to local contributions, accounting for 66% and 82% during the daytime of autumn (6:00-19:00 LT) and summer (5:00-20:00 LT), respectively. However, the contributions of EC-China emissions in daytime O₃ mass increase reached 34% and 18% in two seasons, respectively, indicating the considerable influence of precursor transport on local O₃ photochemistry.

How do transport and photochemistry determine regional O₃ sources in the PRD? Based on the above results, the accumulated morning-hour O₃ mass increase exceeded 10000 t in the PRD for both seasons, which is 6-9 times larger than the original O₃ mass before sunrise (< 1500 t). Thus, daytime O₃ sources within the region were nearly determined by the sources of these newly transported and produced O₃. High contributions of transport, especially the vertical exchange near the ABL top, in O₃ mass changes as well as the dominance of non-local sources in this part of new O₃ ensured that non-local sources contributed to most O₃ in the PRD. Moreover, lower non-local contributions to O₃ in summer than in autumn can be attributed to the combined effects of higher photochemistry contributions in O₃ mass increase, lower non-local contributions in produced O₃ and higher local contributions in transported O₃. Although transport brings massive new O₃ — mostly non-local — into the region in the morning hours, it hardly leads to a drastic increase in O₃ concentration. Thus, transport seems to be less important than photochemistry in the O₃ concentration budget. Therefore, the difference between two O₃ budgets, or the different effects of transport on O₃ concentration and mass, may result in distinct understandings about the role of transport and photochemistry in regional O₃ pollution.

4 Conclusion and outlook

Reported O₃ budgets and source apportionments often concluded with a conflicting role of transport and photochemistry in ambient O₃ pollution. To explore its causes, we used the modelling results of WRF-CMAQ to quantify the contributions of various processes in the O₃ concentration and mass budgets. Results in the PRD revealed that gas-phase chemistry, including daytime photochemistry and night-time O₃ titration, drives the variations of O₃ concentration. Particularly, the former separately contributed to 74% and 95% of O₃ concentration increase in the morning of autumn and summer months. In contrast, transport, especially the vertical exchange near the ABL top, is the main process contributing to the O₃ mass increase in the morning (78% and 53% in autumn and summer, respectively) and its decrease in the afternoon (> 90%). The diurnal changes of transport contributions in two O₃ budgets are closely connected to the variations of ABL and regional

434 wind fields, including the prevailing winds and local circulations (sea breezes), in the PRD. Although massive O₃ transported
435 into the ABL in the morning has a relatively limited influence on O₃ concentration increase (25% and 5% in autumn and
436 summer, respectively) compared to photochemistry, it nearly determines the dominance of non-local sources for daytime O₃
437 in the PRD. The difference between two O₃ budgets, or the different effects of transport on O₃ concentration and mass, may
438 explain why the roles of transport and photochemistry in regional O₃ pollution are inconsistent between different studies.

439

440 It should be noted that the conclusions in this study apply not only to tropospheric O₃ but also to other pollutants with
441 moderately long atmospheric lifetimes, such as some of the secondary components in fine particulate matter. Transport and
442 chemical transformation are both important processes for these pollutants, but for the former, it has different influences on
443 the concentration and mass of pollutants on an hourly scale. Besides regional sources, in theory, the difference between the
444 two budgets may also contribute to the inconsistency of other pollutant characteristics identified using different methods,
445 such as the reaction pathways and sensitivities to precursor emissions. When pollutants with different characteristics are
446 massively transported into the region, the variation of their concentrations is often not notable and thus neglected in the
447 concentration budgets. However, according to the discussions in this study, the transport process is likely to change or even
448 determine the characteristics of pollutants within the region. It also makes the considerable impacts of relatively slow
449 chemistry along the transport on local pollution possible. Therefore, we suggested that attention should be paid to selecting a
450 proper budget type and using correct budget calculation methods in related research.

451

452 Uncertainty remains in the calculated O₃ budgets, which is partly related to the biases in the modelling results. Therefore,
453 supporting observations are essential for future research. Recent progress in observational techniques (Zhao et al., 2021;
454 Zhou et al., 2021) has enabled three-dimensional measurements of meteorological parameters and O₃ concentrations with
455 high spatiotemporal resolution and coverage. These data can be used not only in the model validation of key parameters in
456 budget calculations, but also in the comparisons between observation- and modelling-based contributions by various
457 processes in O₃ budgets. By doing so, more accurate regional-level O₃ budgets will be obtained.

458

459 This study concluded that transport and gas-phase chemistry play the main role in the O₃ concentration and mass budgets,
460 respectively. Based on the two O₃ budgets, we suggest that emission reduction in the upwind regions can effectively lower
461 daily-mean O₃ levels due to its high contributions to regional O₃, but a longer time is needed due to the slow response of O₃
462 concentration to transport. By contrast, reducing local emissions hinders rapid daytime O₃ concentration increase and lowers
463 O₃ peak levels efficiently in the short term. The choice of which strategy to apply should depend on the specific goals of O₃
464 control (mean levels vs. peak levels; long-term vs. short-term), which are set based on a more in-depth understanding of O₃
465 effects on human health, crop yields and ecosystems. More efforts are required to systematically evaluate the effects of
466 different emission reduction strategies on alleviating the detrimental effects of ambient O₃.

467

468 *Data availability.* The source codes of WRF and CMAQ are available at the site
469 https://www2.mmm.ucar.edu/wrf/users/download/get_sources.html and <https://www.cmascenter.org/cmaq/>, respectively.
470 FNL meteorological input files were downloaded from the site <https://rda.ucar.edu/datasets/ds083.2/>. MEIC v1.3
471 anthropogenic emission inventory is available at http://meicmodel.org/?page_id=560. The source codes of MEGAN can be
472 found at <https://bai.ess.uci.edu/megan/data-and-code>. IAGOS dataset used in model validation was searched and downloaded
473 from <http://iagos-data.fr>, which includes all profiles measured in flights taking off from and landing in Hong Kong during
474 two representative months. We also provided the initial Fortran code used in ozone budget calculations and hourly O₃
475 concentration and mass budget results in two representative months (the initial data of Fig. 3) at
476 <https://doi.org/10.5281/zenodo.6259253>.
477
478 *Author contributions.* KQ, XW and YZ designed the study. KQ, XW, TX did the simulations using the WRF-CMAQ model.
479 JS, LZ and YZ provided observational results for model validation. KQ, XW, XC, YY, XJ and YZ developed the post-
480 processing tool, conducted and analysed O₃ budget results. KQ, XW, MV and YZ wrote and revised this paper, with critical
481 feedbacks from all other authors.
482
483 *Competing interests.* The authors declare no conflict of interest.
484
485 *Acknowledgements.* This study was supported by the National Key Research and Development Program of China (grant No.
486 2018YFC0213204), the National Science and Technology Pillar Program of China (grant No. 2014BAC21B01) and the co-
487 funded DFG-NSFC Sino-German AirChanges project (grant No. 448720203).
488

489 **References**

- 490 Ainsworth, E. A.: Understanding and improving global crop response to ozone pollution, *Plant J.*, 90, 886–897,
491 <https://doi.org/10.1111/tpj.13298>, 2017.
- 492 Bates, K. H. and Jacob, D. J.: An expanded definition of the odd oxygen family for tropospheric ozone budgets: Implications
493 for ozone lifetime and stratospheric influence, *Geophys. Res. Lett.*, 47, e2019GL084486,
494 <https://doi.org/10.1029/2019GL084486>, 2019.
- 495 Boian, C. and Andrade, M. D. F.: Characterization of ozone transport among metropolitan regions, *Rev. Bras. Meteorol.*, 27,
496 229–242, <https://doi.org/10.1590/S0102-77862012000200009>, 2012.
- 497 Chang, X., Wang, S., Zhao, B., Cai, S., and Hao, J.: Assessment of inter-city transport of particulate matter in the Beijing–
498 Tianjin–Hebei region, *Atmos. Chem. Phys.*, 18, 4843–4858, <https://doi.org/10.5194/acp-18-4843-2018>, 2018.
- 499 Clappier, A., Belis, C. A., Pernigotti, D., and Thunis, P.: Source apportionment and sensitivity analysis: two methodologies
500 with two different purposes, *Geosci. Model Dev.*, 10, 4245–4256, <https://doi.org/10.5194/gmd-10-4245-2017>, 2017.
- 501 Ding, A., Wang, T., Zhao, M., Wang, T. J., and Li, Z. K.: Simulation of sea-land breezes and a discussion of their
502 implications on the transport of air pollution during a multi-day ozone episode in the Pearl River Delta of China,
503 *Atmos. Environ.*, 38, 6737–6750, <https://doi.org/10.1016/j.atmosenv.2004.09.017>, 2004.
- 504 Fishman, J., Wozniak, A. E., and Creilson, J. K.: Global distribution of tropospheric ozone from satellite measurements
505 using the empirically corrected tropospheric ozone residual technique: Identification of the regional aspects of air
506 pollution, *Atmos. Chem. Phys.*, 3, 893–907, <https://doi.org/10.5194/acp-3-893-2003>, 2003.
- 507 Fleming, Z. L., Doherty, R. M., von Schneidemesser, E., Malley, C. S., Cooper, O. R., Pinto, J. P., Colette, A., Xu, X. B.,
508 Simpson, D., Schultz, M. G., Lefohn, A. S., Hamad, S., Moolla, R., Solberg, S., and Feng, Z. Z.: Tropospheric ozone
509 assessment report: Present-day ozone distribution and trends relevant to human health, *Elementa-Sci. Anthropol.*, 6, 12,
510 <https://doi.org/10.1525/elementa.273>, 2018.
- 511 Fowler, D., Brimblecombe, P., Burrows, J., Heal, M. R., Grennfelt, P., Stevenson, D. S., Jowett, A., Nemitz, E., Coyle, M.,
512 Liu, X., Chang, Y., Fuller, G. W., Sutton, M. A., Klimont, Z., Unsworth, M. H., and Vieno, M.: A chronology of global
513 air quality, *Philos. T. R. Soc. A*, 378, 20190314, <https://doi.org/10.1098/rsta.2019.0314>, 2020.
- 514 Gao, M., Gao, J., Zhu, B., Kumar, R., Lu, X., Song, S., Zhang, Y., Jia, B., Wang, P., Beig, G., Hu, J., Ying, Q., Zhang, H.,
515 Sherman, P., and McElroy, M. B.: Ozone pollution over China and India: seasonality and sources, *Atmos. Chem. Phys.*,
516 20, 4399–4414, <https://doi.org/10.5194/acp-20-4399-2020>, 2020.
- 517 Gao, X., Deng, X., Tan, H., Wang, C., Wang, N., and Yue, D.: Characteristics and analysis on regional pollution process and
518 circulation weather types over Guangdong Province, *Acta Scientiae Circumstantiae* (in Chinese), 38(5), 1708–1716,
519 <https://doi.org/10.13671/j.hjkxxb.2017.0473>, 2018.

520 Guo, J. J., Fiore, A. M., Murray, L. T., Jaffe, D. A., Schnell, J. L., Moore, C. T., and Milly, G. P.: Average versus high
 521 surface ozone levels over the continental USA: model bias, background influences, and interannual variability, *Atmos.*
 522 *Chem. Phys.*, 18, 12123–12140, <https://doi.org/10.5194/acp-18-12123-2018>, 2018.

523 Hou, X., Zhu, B., Kang, H., and Gao, J.: Analysis of seasonal ozone budget and spring ozone latitudinal gradient variation in
 524 the boundary layer of the Asia-Pacific region, *Atmos. Environ.*, 94, 734–741,
 525 <https://doi.org/10.1016/j.atmosenv.2014.06.006>, 2014.

526 Hu, J., Li, Y., Zhao, T., Liu, J., Hu, X.-M., Liu, D., Jiang, Y., Xu, J., and Chang, L.: An important mechanism of regional O₃
 527 transport for summer smog over the Yangtze River Delta in eastern China, *Atmos. Chem. Phys.*, 18, 16239–16251,
 528 <https://doi.org/10.5194/acp-18-16239-2018>, 2018.

529 Janssen, R. H. H. and Pozzer, A.: Description and implementation of a MiXed Layer model (MXL, v1.0) for the dynamics of
 530 the atmospheric boundary layer in the Modular Earth Submodel System (MESSy), *Geosci. Model Dev.*, 8, 453–471,
 531 <https://doi.org/10.5194/gmd-8-453-2015>, 2015.

532 Jin, X., Cai, X., Huang, Q., Wang, X., Song, Y., and Zhu, T.: Atmospheric boundary layer—free troposphere air exchange in
 533 the North China Plain and its impact on PM_{2.5} pollution, *J. Geophys. Res.-Atmos.*, 126(9), e2021JD034641,
 534 <https://doi.org/10.1029/2021JD034641>, 2021.

535 Kaser, L., Patton, E. G., Pfister, G. G., Weinheimer, A. J., Montzka, D. D., Flocke, F., Thompson, A. M., Stauffer, R. M.,
 536 and Halliday, H. S.: The effect of entrainment through atmospheric boundary layer growth on observed and modeled
 537 surface ozone in the Colorado Front Range, *J. Geophys. Res.-Atmos.*, 122, 6075–6093,
 538 <https://doi.org/10.1002/2016JD026245>, 2017.

539 Kulmala, M., Kokkonen, T. V., Pekkanen, J., Paatero, S., Petäjä, T., Kerminen, V.-M., and Ding, A.: Opinion: Gigacity – a
 540 source of problems or the new way to sustainable development, *Atmos. Chem. Phys.*, 21, 8313–8322,
 541 <https://doi.org/10.5194/acp-21-8313-2021>, 2021.

542 Lee, X.: *Fundamentals of Boundary-Layer Meteorology*, Springer Atmospheric Sciences., 2018.

543 Lelieveld, J., Hoor, P., Jöckel, P., Pozzer, A., Hadjinicolaou, P., Cammas, J.-P., and Beirle, S.: Severe ozone air pollution in
 544 the Persian Gulf region, *Atmos. Chem. Phys.*, 9, 1393–1406, <https://doi.org/10.5194/acp-9-1393-2009>, 2009.

545 Lenschow, D. H., Pearson, R., and Stankov, B. B.: Estimating the ozone budget in the boundary layer by use of aircraft
 546 measurements of ozone eddy flux and mean concentration, *J. Geophys. Res.*, 86, 7291–7297,
 547 <https://doi.org/10.1029/JC086iC08p07291>, 1981.

548 Li, A., Zhou, Q., and Xu, Q.: Prospects for ozone pollution control in China: An epidemiological perspective, *Environ.*
 549 *Pollut.*, 285, 117670, <https://doi.org/10.1016/j.envpol.2021.117670>, 2021b.

550 Li, L., Xie, F., Li, J., Gong, K., Xie, X., Qin, Y., Qin, M., and Hu, J.: Diagnostic analysis of regional ozone pollution in
 551 Yangtze River Delta, China: A case study in summer 2020, *Sci. Total Environ.*, 812, 151511,
 552 <https://doi.org/10.1016/j.scitotenv.2021.151511>, 2021a.

553 Li, Y., Lau, A. K. H., Fung, J. C. H., Ma, H., and Tse, Y.: Systematic evaluation of ozone control policies using an Ozone
 554 Source Apportionment method, *Atmos. Environ.*, 76, 136–146, <https://doi.org/10.1016/j.atmosenv.2013.02.033>, 2013.

555 Li, Y., Lau, A. K. H., Fung, J. C. H., Zheng, J. Y., Zhong, L. J., and Louie, P. K. K.: Ozone source apportionment (OSAT) to
 556 differentiate local regional and super-regional source contributions in the Pearl River Delta region, China, *J. Geophys.*
 557 *Res.-Atmos.*, 117, D15305, <http://doi.org/10.1029/2011JD017340>, 2012.

558 Liu, H. L., Zhang, M. G., and Han, X.: A review of surface ozone source apportionment in China, *Atmos. Ocean. Sci. Lett.*,
 559 13, 470–484, <https://doi.org/10.1080/16742834.2020.1768025>, 2020.

560 Liu, P., Zhang, Y., Yu, S. C., and Schere, K. L.: Use of a Process Analysis tool for diagnostic study on fine particulate matter
 561 predictions in the U.S. Part II: Process Analysis and sensitivity simulations, *Atmos. Pollut. Res.*, 2, 61–71,
 562 <https://doi.org/10.5094/APR.2011.008>, 2011.

563 Lu, X., Hong, J., Zhang, L., Cooper, O. R., Schultz, M. G., Xu, X., Wang, T., Gao, M., Zhao, Y., and Zhang, Y.: Severe
 564 surface ozone pollution in China: A global perspective, *Environ. Sci. Tech. Lett.*, 5(8), 487–494,
 565 <https://doi.org/10.1021/acs.estlett.8b00366>, 2018.

566 Massagué, J., Carnerero, C., Escudero, M., Baldasano, J. M., Alastuey, A., and Querol, X.: 2005–2017 ozone trends and
 567 potential benefits of local measures as deduced from air quality measurements in the north of the Barcelona
 568 metropolitan area, *Atmos. Chem. Phys.*, 19, 7445–7465, <https://doi.org/10.5194/acp-19-7445-2019>, 2019.

569 Mills, G., Wagg, S., and Harmens, H.: Ozone pollution: impacts on ecosystem services and biodiversity (CEH Project no.
 570 C04062, C04325), Bangor, UK, NERC/Centre for Ecology & Hydrology, 2013.

571 Naik, V., Szopa, S., Adhikary, B., Artaxo, P., Berntsen, T., Collins, W. D., Fuzzi, S., Gallardo, L., Kiendler Scharr, A.,
 572 Klimont, Z., Liao, H., Unger, N., and Zanis, P.: Short-Lived Climate Forcers, in: *Climate Change 2021: The Physical*
 573 *Science Basis. Contribution of Working Group I to the Sixth Assessment Report of the Intergovernmental Panel on*
 574 *Climate Change*, edited by: Masson-Delmotte, V., Zhai, P., Pirani, A., Connors, S. L., Péan, C., Berger, S., Caud, N.,
 575 Chen, Y., Goldfarb, L., Gomis, M. I., Huang, M., Leitzell, K., Lonnoy, E., Matthews, J. B. R., Maycock, T. K.,
 576 Waterfield, T., Yelekçi, O., Yu, R., and Zhou, B., Cambridge University Press, Cambridge, United Kingdom and New
 577 York, NY, USA, 817–922, <https://doi.org/10.1017/9781009157896.008>, 2021.

578 Novel, D. P.: The OTC challenge: Adding VOC controls in the northeast, *J. Air Waste Manag. Assoc.*, 42(8), 1053–1056,
 579 <https://doi.org/10.1080/10473289.1992.10467050>, 1992.

580 Pay, M. T., Gangoiti, G., Guevara, M., Napelenok, S., Querol, X., Jorba, O., and Pérez García-Pando, C.: Ozone source
 581 apportionment during peak summer events over southwestern Europe, *Atmos. Chem. Phys.*, 19, 5467–5494,
 582 <https://doi.org/10.5194/acp-19-5467-2019>, 2019.

583 Petzold, A., Thouret, V., Gerbig, C., Zahn, A., Brenninkmeijer, C. A. M., Gallagher, M., Hermann, M., Pontaud, M., Ziereis,
 584 H., Boulanger, D., Marshall, J., Nédélec, P., Smit, H. G. J., Friess, U., Flaud, J.-M., Wahner, A., Cammas, J.-P., Volz-
 585 Thomas, A. and IAGOS TEAM: Global-scale atmosphere monitoring by in-service aircraft—current achievements and

586 future prospects of the European Research Infrastructure IAGOS, *Tellus B*, 67, 28452,
587 <https://doi.org/10.3402/tellusb.v67.28452>, 2015.

588 Qu, K., Wang, X., Yan, Y., Shen, J., Xiao, T., Dong, H., Zeng, L., and Zhang, Y.: A comparative study to reveal the
589 influence of typhoons on the transport, production and accumulation of O₃ in the Pearl River Delta, China, *Atmos.*
590 *Chem. Phys.*, 21, 11593–11612, <https://doi.org/10.5194/acp-21-11593-2021>, 2021.

591 Reid, N., Yap, D., and Bloxam, R.: The potential role of background ozone on current and emerging air issues: An overview,
592 *Air Qual. Atmos. Health*, 1, 19–29, <https://doi.org/10.1007/s11869-008-0005-z>, 2008.

593 Schultz, M. G., Schröder, S., Lyapina, O., Cooper, O., Galbally, I., Petropavlovskikh, I., Von Schneidemesser, E., Tanimoto,
594 H., Elshorbany, Y., Naja, M., Seguel, R., Dauert, U., Eckhardt, P., Feigenspahn, S., Fiebig, M., Hjellbrekke, A.-G.,
595 Hong, Y.-D., Kjeld, P. C., Koide, H., Lear, G., Tarasick, D., Ueno, M., Wallasch, M., Baumgardner, D., Chuang, M.-T.,
596 Gillett, R., Lee, M., Molloy, S., Moolla, R., Wang, T., Sharps, K., Adame, J. A., Ancellet, G., Apadula, F., Artaxo, P.,
597 Barlasina, M., Bogucka, M., Bonasoni, P., Chang, L., Colomb, A., Cuevas, E., Cupeiro, M., Degorska, A., Ding, A.,
598 Fröhlich, M., Frolova, M., Gadhavi, H., Gheusi, F., Gilge, S., Gonzalez, M. Y., Gros, V., Hamad, S. H., Helmig, D.,
599 Henriques, D., Hermansen, O., Holla, R., Huber, J., Im, U., Jaffe, D. A., Komala, N., Kubistin, D., Lam, K.-S., Laurila,
600 T., Lee, H., Levy, I., Mazzoleni, C., Mazzoleni, L., McClure-Begley, A., Mohamad, M., Murovic, M., Navarro-Comas,
601 M., Nicodim, F., Parrish, D., Read, K. A., Reid, N., Ries, L., Saxena, P., Schwab, J. J., Scorgie, Y., Senik, I.,
602 Simmonds, P., Sinha, V., Skorokhod, A., Spain, G., Spangl, W., Spoor, R., Springston, S. R., Steer, K., Steinbacher, M.,
603 Suharguniyawan, E., Torre, P., Trickl, T., Weili, L., Weller, R., Xu, X., Xue, L., and Zhiqiang, M.: Tropospheric ozone
604 assessment report: Database and metrics data of global surface ozone observations, *Elementa-Sci. Anthropol.*, 5, 58,
605 <https://doi.org/10.1525/elementa.244>, 2017.

606 Sinclair, V. A., Belcher, S. E., and Gray, S. L.: Synoptic controls on boundary-layer characteristics, *Bound.-Layer Meteorol.*,
607 134, 387–409, <https://doi.org/10.1007/s10546-009-9455-6>, 2010.

608 Sitch, S., Cox, P. M., Collins, W. J., and Huntingford, C.: Indirect radiative forcing of climate change through ozone effects
609 on the land-carbon sink, *Nature*, 448, 791–795, <https://doi.org/10.1038/nature06059>, 2007.

610 Stevenson, D. S., Dentener, F. J., Schultz, M. G., Ellingsen, K., van Noije, T. P. C., Wild, O., Zeng, G., Amann, M.,
611 Atherton, C. S., Bell, N., Bergmann, D. J., Bey, I., Butler, T., Cofala, J., Collins, W. J., Derwent, R. G., Doherty, R. M.,
612 Drevet, J., Eskes, H. J., Fiore, A. M., Gauss, M., Hauglustaine, D. A., Horowitz, L. W., Isaksen, I. S. A., Krol, M. C.,
613 Lamarque, J.-F., Lawrence, M. G., Montanaro, V., Müller, J.-F., Pitari, G., Prather, M. J., Pyle, J. A., Rast, S.,
614 Rodriguez, J. M., Sanderson, M. G., Savage, N. H., Shindell, D. T., Strahan, S. E., Sudo, K., and Szopa, S.: Multimodel
615 ensemble simulations of present-day and near-future tropospheric ozone, *J. Geophys. Res.*, 111, D08301,
616 <https://doi.org/10.1029/2005JD006338>, 2006.

617 Su, R., Lu, K. D., Yu, J. Y., Tan, Z. F., Jiang, M. Q., Li, J., Xie, S. D., Wu, Y. S., Zeng, L. M., Zhai, C. Z., and Zhang, Y. H.:
618 Exploration of the formation mechanism and source attribution of ambient ozone in Chongqing with an observation-
619 based model, *Sci. China Earth Sci.*, 61, 23–32, <https://doi.org/10.1007/s11430-017-9104-9>, 2018.

620 Tan, Z., Lu, K., Jiang, M., Su, R., Dong, H., Zeng, L., Xie, S., Tan, Q., and Zhang, Y.: Exploring ozone pollution in
621 Chengdu, southwestern China: A case study from radical chemistry to O₃-VOC-NO_x sensitivity, *Sci. Total Environ.*,
622 636, 775–786, <https://doi.org/10.1016/j.scitotenv.2018.04.286>, 2018.

623 Tan, Z., Lu, K., Jiang, M., Su, R., Wang, H., Lou, S., Fu, Q., Zhai, C., Tan, Q., Yue, D., Chen, D., Wang, Z., Xie, S., Zeng,
624 L., and Zhang, Y.: Daytime atmospheric oxidation capacity in four Chinese megacities during the photochemically
625 polluted season: a case study based on box model simulation, *Atmos. Chem. Phys.*, 19, 3493–3513,
626 <https://doi.org/10.5194/acp-19-3493-2019>, 2019.

627 Tang, G., Liu, Y., Huang, X., Wang, Y., Hu, B., Zhang, Y., Song, T., Li, X., Wu, S., Li, Q., Kang, Y., Zhu, Z., Wang, M.,
628 Wang, Y., Li, T., Li, X., and Wang, Y.: Aggravated ozone pollution in the strong free convection boundary layer, *Sci.*
629 *Total Environ.*, 788, 147740, <https://doi.org/10.1016/j.scitotenv.2021.147740>, 2021.

630 Tang, G. Q., Zhu, X. W., Xin, J. Y., Hu, B., Song, T., Sun, Y., Zhang, J. Q., Wang, L. L., Cheng, M. T., Chao, N., Kong, L.
631 B., Li, X., and Wang, Y. S.: Modelling study of boundary-layer ozone over northern China – Part I: Ozone budget in
632 summer, *Atmos. Res.*, 187, 128–137, <https://doi.org/10.1016/j.atmosres.2016.10.017>, 2017.

633 Thunis, P., Clappier, A., Tarrason, L., Cuvelier, C., Monteiro, A., Pisoni, E., Wesseling, J., Belis, C. A., Pirovano, G.,
634 Janssen, S., Guerreiro, C., and Peduzzi, E.: Source apportionment to support air quality planning: Strengths and
635 weaknesses of existing approaches, *Environ. Int.*, 130, 104825, <https://doi.org/10.1016/j.envint.2019.05.019>, 2019.

636 Trousdell, J. F., Caputi, D., Smoot, J., Conley, S. A., and Faloona, I. C.: Photochemical production of ozone and emissions
637 of NO_x and CH₄ in the San Joaquin Valley, *Atmos. Chem. Phys.*, 19, 10697–10716, [https://doi.org/10.5194/acp-19-](https://doi.org/10.5194/acp-19-10697-2019)
638 10697-2019, 2019.

639 Trousdell, J. F., Conley, S. A., Post, A., and Faloona, I. C.: Observing entrainment mixing, photochemical ozone production,
640 and regional methane emissions by aircraft using a simple mixed-layer framework, *Atmos. Chem. Phys.*, 16, 15433–
641 15450, <https://doi.org/10.5194/acp-16-15433-2016>, 2016.

642 Vilà-Guerau De Arellano, J., van Heerwaarden, C. C., van Stratum, B. J. H., and van den Dries, K.: *Atmospheric Boundary*
643 *Layer: Integrating Air Chemistry and Land Interactions*, Cambridge University Press, New York, 2015.

644 Yan, F., Gao, Y., Ma, M., Liu, C., Ji, X., Zhao, F., Yao, X., and Gao, H.: Revealing the modulation of boundary conditions
645 and governing processes on ozone formation over northern China in June 2017, *Environ. Pollut.*, 272, 115999,
646 <https://doi.org/10.1016/j.envpol.2020.115999>, 2021.

647 Yang, L., Wang, X., and Chen, Q.: New method for investigating regional interactions of air pollutants (in Chinese), *Acta*
648 *Sci. Circumstantiae*, 32(3), 528–536, <https://doi.org/10.13671/j.hjkxxb.2012.03.012>, 2012.

649 Yang, W., Chen, H., Wang, W., Wu, J., Li, J., Wang, Z., Zheng, J., and Chen, D.: Modeling study of ozone source
650 apportionment over the Pearl River Delta in 2015, *Environ. Pollut.*, 253, 393–402,
651 <https://doi.org/10.1016/j.envpol.2019.06.091>, 2019.

652 You, C., and Fung, J. C. H.: Characteristics of the sea-breeze circulation in the Pearl River Delta region and its dynamical
653 diagnosis. *Journal of Applied Meteorology and Climatology*, 58(4), 741-755, [https://doi.org/10.1175/JAMC-D-18-](https://doi.org/10.1175/JAMC-D-18-0153.1)
654 0153.1, 2019.

655 Yu, D., Tan, Z., Lu, K., Ma, X., Li, X., Chen, S., Zhu, B., Lin, L., Li, Y., Qiu, P., Yang, X., Liu, Y., Wang, H., He, L.,
656 Huang, X., and Zhang, Y.: An explicit study of local ozone budget and NO_x-VOCs sensitivity in Shenzhen China,
657 *Atmos. Environ.*, 224, 117304, <https://doi.org/10.1016/j.atmosenv.2020.117304>, 2020.

658 Zhang, J. J., Wei, Y., and Fang, Z.: Ozone pollution: A major health hazard worldwide, *Front. Immunol.*, 10, 2518,
659 <https://doi.org/10.3389/fimmu.2019.02518>, 2019.

660 Zhao, R., Hu, Q., Sun, Z., Wu, Y., Xing, C., Liu, H., and Liu, C., (2021). Review of space and ground integrated remote
661 sensing for air pollutants (in Chinese). *Res. Environ. Sci.*, 34(1), 28-40. [https://doi.org/10.13198/j.issn.1001-](https://doi.org/10.13198/j.issn.1001-6929.2020.11.25)
662 6929.2020.11.25, 2021.

663 Zhao, W., Tang, G., Yu, H., Yang, Y., Wang, Y., Wang, L., An, J., Gao, W., Hu, B., Cheng, M., An, X., Li, X., and Wang,
664 Y.: Evolution of boundary layer ozone in Shijiazhuang, a suburban site on the North China Plain, *J. Environ. Sci.*, 83,
665 152–160, <https://doi.org/10.1016/j.jes.2019.02.016>, 2019.

666 Zhou, B., Zhang, S., Xue, R., Li, J., and Wang, S.: A review of Space-Air-Ground integrated remote sensing techniques for
667 atmospheric monitoring, *J. Environ. Sci.*, <https://doi.org/10.1016/j.jes.2021.12.008>, 2021.

668